Journal of Solid State Chemistry 183 (2010) 1776–1784

Contents lists available at ScienceDirect

Journal of Solid State Chemistry

journal homepage: www.elsevier.com/locate/jssc

Characterizing CA_2 and CA_6 using ELNES

A. Altay [a,1], C.B. Carter [b,*,1], P. Rulis [c], W.-Y. Ching [c], I. Arslan [d], M.A. Gülgün [e]

[a] Envy, Energy and Environmental Investments, Inc., Ankara 06450, Turkey
[b] Department of Chemical, Materials and Biomolecular Engineering, University of Connecticut, Storrs, CT 06269-3222, USA
[c] Department of Physics, University of Missouri-Kansas City, Kansas City, MO 64110, USA
[d] University of California, Davis, CA 95616, USA
[e] Sabanci University, FENS, Orhanli, Tuzla, 34956 Istanbul, Turkey

ARTICLE INFO

Article history:
Received 29 December 2008
Received in revised form
20 April 2010
Accepted 22 May 2010
Available online 27 May 2010

Keywords:
Calcium aluminates
ELNES
STEM
TEM
Ab initio calculations
EELS
X-ray diffraction

ABSTRACT

Calcium aluminates, compounds in the $CaO–Al_2O_3$ phase system, are used in high-temperature cements and refractory oxides and have wide range of potential technological applications due to their interesting optical, electrical, thermal, and mechanical properties. They are used in both crystalline and glassy form; the glass is an isotropic material while the crystalline materials may be highly anisotropic. This paper will consider two particular crystalline materials, CA_2 and CA_6, but the results should be applicable to all calcium aluminates. Although CA_2 and CA_6 crystals contain the same chemical species, Ca, Al, and O, the coordination and local environments of these species are different in the two structures and hence they show very different energy-loss near-edge structures (ELNES) when examined by electron energy-loss spectroscopy (EELS) in the TEM. The data obtained using ELNES can effectively provide a fingerprint for each compound and a map for their electronic structure. Once such fingerprints are obtained, they can be used to identify nano-sized particles/grains or material at interfaces and grain boundaries.

In the present study, the local symmetry fingerprints for CA_2 and CA_6 structures are reported combining experimental spectra with electronic-structure calculations that allow the different features in the spectra to be interpreted. Al-$L_{2,3}$ and O-K edge core-loss spectra from CA_2 and CA_6 were measured experimentally using electron energy-loss spectroscopy in a monochromated scanning transmission electron microscope. The near-edge structures were calculated for the different phases using the orthogonalized linear combination of atomic-orbitals method, and took account of core–hole interactions. It is shown that CA_2 and CA_6 structures exhibit distinctive experimental ELNES fingerprints so that these two phases can be separately identified even when present in small volumes.

1. Introduction

Although the binary compounds of the $CaO–Al_2O_3$ system have long been used in high-temperature cements [1] and refractory oxides [2], they also have a wide range of potential technological applications due to their optical, electrical, thermal, and mechanical properties. Calcium aluminate glasses are attractive candidates for low-loss optical fibers [3]. They transmit electromagnetic radiation moderately far [4] into the infrared region (25% at 5.5 μm for a 2 mm optical path) [5] and they are photosensitive [6]. Crystalline $CaAl_4O_7$ ($CaO \cdot 2Al_2O_3$, CA_2) has a very low coefficient of thermal expansion ($1.2 \times 10^6\ K^{-1}$ up to 372 K [7]) and thus, it has been used as a thermal-shock-resistant refractory material. Crystalline $CaAl_{12}O_{19}$ ($CaO \cdot 6Al_2O_3$, CA_6) [8] is a known interface phase in fiber-reinforced ceramic-oxide composites that facilitates the fiber pull-out and improves the strength of the material [9]. Lacerda et al. [10] reported that $Ca_{12}Al_{14}O_{33}$ ($12CaO \cdot 7Al_2O_3$, $C_{12}A_7$) is an ion conductor at high temperatures. More recently, Hayashi et al. [11] reported that when hydrogen is incorporated, $C_{12}A_7$ can be converted from an electrical insulator into an electrical conductor by UV-light illumination.

Despite the growing technological importance of calcium aluminate phases, there have been a limited number of studies of their crystallographic and electronic structure. Early crystallographic investigations were carried out using various XRD techniques [12–17]. More recently, multinuclear solid-state NMR studies have reported the structure and atomic environment of these phases [18,19]. Undoubtedly, most illuminating studies of the electronic structure of calcium aluminates resulted from XANES were reported by Weigel et al. [20] and Henderson et al. [21] in the past few years using SGM beamline at the Canadian Light Source (CLS).

* Corresponding author. Fax: +1 860 486 2959.
E-mail address: cbcarter@engr.uconn.edu (C.B. Carter).
[1] Previously at: Department of Chemical Engineering and Materials Science, University of Minnesota, Minneapolis, MN 55455, USA.

0022-4596/$ - see front matter © 2010 Elsevier Inc. All rights reserved.
doi:10.1016/j.jssc.2010.05.028

It is not trivial to calculate the electronic structures of calcium aluminate phases theoretically due to the large and complicated structures of these phases. Previously, theoretical calculation of the electronic structure of $CaAl_2O_4$ (CA) has been reported [22]; however, until this study theoretical calculations of the electronic structures of CA_2 and CA_6 including the core–hole interactions have not been reported. In this paper, electron energy-loss spectroscopy in the TEM has been combined with calculations of the electronic structure to provide a method for identifying these phases when other techniques are problematic.

2. Materials and methods

2.1. Calcium di-aluminate ($CaAl_4O_7$, $CaO \cdot 2Al_2O_3$, CA_2)

The occurrence of $CaO \cdot 2Al_2O_3$ was initially reported by two independent studies in 1937 [23,24]. Goldsmith [25], and Goria and Burdese [26] stated that CA_2 is monoclinic according to X-ray diffraction results, but Goldsmith's optical properties indicated that the compound should be either hexagonal or tetragonal. Filonenko and Laurov [27] reported that CA_2 crystallizes in the tetragonal state. Controversy over the exact crystal structure of the CA_2 was not resolved for many years. Boyko and Wisnyi [17] reported that CA_2 forms a monoclinic crystal with a space group $C2/c$; Cockayne and Robertson [15] concluded that this phase is complex hexagonal. Goodwin and Lindop [16] confirmed the monoclinic structure and the results reported in that study are now the accepted crystal data for CA_2. Structural data for CA_2 and the atomic positions in the crystal are listed in Tables 1 and 2, respectively.

2.2. Calcium hexa-aluminate ($CaAl_{12}O_{19}$, $CaO \cdot 6Al_2O_3$, CA_6)

CA_6 is a stable aluminate found at the alumina-rich end of the binary phase diagram [28]. It also occurs in nature as the mineral hibonite. (Paul Hibon discovered the mineral in 1956 [29].)

The crystal structure of CA_6 was studied by Kato and Saalfeld [30], and confirmed to be isostructural with the mineral magnetoplumbite (MP) [12,31]. CA_6 belongs to the hexagonal space group $P6_3/mmc$ and can be represented symbolically as $CaAlO_3[Al_{11}O_{16}]$. The portion in brackets represents the spinel block and the remainder is the inter-spinel layer. In the CA_6 structure, the Ca ions are dodecahedrally (12-fold) coordinated in the inter-spinel layer. Al ions are distributed over three crystallographically independent octahedral sites, one tetrahedral site, and one bi-pyramidal site. The exact location of the Al atom in the trigonal bi-pyramidal site was first explained using the split-atom model [13] (see also [32]). It was shown that the Al^{3+} ion statistically occupies one of the two equivalent sites displaced from the mirror plane [13]. Structural data for the CA_6 crystal and the atomic positions with coordination values are given in Tables 3 and 4, respectively.

Table 1
Structural information for CA_2 [16].

Formula: $CaO \cdot 2Al_2O_3$	**Lattice parameters**
Space group: $C2/c$	$a=12.8398$ Å
Volume: 591.54 Å^3	$b=8.8624$ Å
No. of formula units/unit cell: 4	$c=5.4311$ Å
Density: 2.915 g cm^{-3}	$\alpha=\gamma=90^\circ$, $\beta=106^\circ$

Table 2
Atomic positions for CA_2 [16].

Atom	**Position (Wyckoff)**	**Coordination**	***x***	***y***	***z***
Al(1)	8*f*	4	0.16410	0.08670	0.30300
Al(2)	8*f*	4	0.11980	0.44060	0.24100
Ca	4*e*	6[a]	0	0.80910	0.25000
O(1)	4*e*	4 Al	0	0.52310	0.25000
O(2)	8*f*	2 Al+2 Ca	0.11550	0.05120	0.56590
O(3)	8*f*	2 Al+1 Ca	0.11850	0.25530	0.14910
O(4)	8*f*	3 Al	0.19240	0.44360	0.57970

[a] Although the Ca coordination is known to be 7 in CA_2 crystal, based on the bond-length criteria used for the interpretation of the data in this study Ca coordination is listed as 6-fold.

Table 3
Structural information for CA_6 [13].

Formula: $CaO \cdot 6Al_2O_3$	**Lattice parameters**
Space group: $P6_3/mmc$	$a=5.5587$ Å
Volume: 585.83 Å^3	$b=21.8929$ Å
No. of formula units/unit cell: 2	$\alpha=\beta=90^\circ$
Density: 3.79 g cm^{-3}	$\gamma=120^\circ$

2.3. Structural investigations using ELNES

The low-energy portion of the electron energy-loss spectrum (EELS) is known by the acronym ELNES (energy-loss near-edge structure). ELNES is sensitive to the density of unoccupied states (DOS) above the Fermi energy (E_F) around the central atom [8,33–36]. The energy level of the unoccupied states is strongly influenced by the interaction of the central atom with its close neighbors. Therefore, ELNES can provide information about the structural and chemical properties of the atom undergoing excitation. It can thus be used as a probe of the bonding and nearest-neighbor coordination, and therefore the local symmetry [37,38]. These near edge structures are also sensitive to the valence state of the excited atom [39,40]. The combination of these information makes ELNES a technique that provides a fingerprint of a particular crystal structure.

An unsurpassed advantage of EELS/STEM combination over other analytical techniques is its sub-nanometer spatial resolution. This advantage allows the fingerprinting by the ELNES method in order to identify the structure of the small feature being probed by the STEM. The methodology behind this technique should be supported by both systematic measurements on suitable reference materials, and by electronic calculations [22,41]. This combination of experimental study and theoretical calculation which gives the fingerprint, can then help to identify the local bonding in unknown phases and can be associated with spatially localized structural features such as interfaces and defects [42,43].

When the ELNES fingerprints of two different coordinations of the same element have been determined, it is, in principle, possible to use these fingerprints to analyze compounds where both coordinations coexist and thus to determine the relative site occupancies via an algorithm or fitting procedure. This technique has mainly been applied to light elements to determine the proportion of sp^2-bonded carbon atoms in amorphous diamond films [44,45] and the proportion of BO_3 and BO_4 groups in various compounds containing boron–oxygen polyhedra [46]. The possibility of using Al K- and Al $L_{2,3}$-ELNES fingerprints to extract the site occupancies in mixed-coordination materials has also been investigated [47].

Table 4
Atomic positions for CA_6 [13].

Atom	Position (Wyckoff)	Coordination	x	y	z
Al(1)	2a	6	0	0	0
Al(2)	4e	4[a]	0	0	0.25771
Al(3)	4f	4	0.33333	0.66667	0.02808
Al(4)	4f	6	0.33333	0.66667	0.19102
Al(5)	12k	6	0.16855	0.33710	0.89086
Ca	2d	12	0.66667	0.33333	0.25000
O(1)	4e	4 Al	0	0	0.14907
O(2)	4f	4 Al	0.66667	0.33333	0.05461
O(3)	6h	4 Al+2 Ca	0.18107	0.36214	0.25000
O(4)	12k	4 Al	0.15505	0.31010	0.05213
O(5)	12k	3 Al+1 Ca	0.50325	0.00650	0.14912

[a] Al(2) is in the trigonal bi-pyramidal site which has 5-fold coordination. Based on the bond-length criteria used for the interpretation of the data in this study, one of the bonds between Al(2)–O(1) is longer than 2.20 Å. Therefore, the Al(2) coordination is listed as 4-fold.

ELNES is also sensitive to the variations in bond lengths and bond angles. Comparison of experimentally observed spectra with those derived from standards, together with theoretical calculations, can yield a measure of the distortion in a material such as variations in bond lengths and bond angles [48].

2.4. Ab initio calculations using OLCAO

Many attempts have been made to compare measured ELNES with calculations of the density of states. A reasonable understanding of ELNES has been established using inelastic electron scattering theory [33,49]. Two approaches have been used to compute ELNES and X-ray absorption near-edge structures (XANES) (the X-ray equivalent to ELNES); the two calculations are each essentially two ways to produce the same calculation of the local electronic structure.

The first approach takes account of multiple-scattering to compute the scattering of the excited electron associated with X-ray absorption [50,51]. This approach is a standard technique for analyzing extended X-ray absorption fine structure (EXAFS), which involves closely related parameters [52,53]. Proper selection of computational parameters such as the number of scattered waves, the shape of the scattering potentials, the size of the cluster model, etc., are critical in reproducing the data present in quantitative experimental measurements of near-edge features.

The second approach uses electronic band-structure methods with periodic boundary conditions [54,55]. One such band-structure method is the orthogonalized linear combination of atomic orbitals (OLCAO) method that uses atomic orbitals expressed by a set of Gaussian functions [56]. The OLCAO method is an *ab initio* electron band-structure method based on density functional theory.

The local density of states (LDOS) obtained from the OLCAO calculation has been used to interpret the ELNES spectra of several oxides including some containing grain boundaries [41,57,58]. However, the addition of a core–hole effect is necessary for a more precise analysis. The core–hole effect originates with the Coulomb interaction between the positively charged core–hole and the excited electron in the conduction band; the excited atom undergoes an electronic relaxation, which must be taken into account in the calculation. This effect can be successfully computed by including a core–hole into the self-consistent calculations using a super-cell model [59]. In this approach, the initial state is the ground state of the super-cell containing the core levels of the targeted atom; the final state (the core–hole state) is modeled by removing an electron from the core orbital (1s for the K edge, 2p for the L edge) and moving it to the bottom of the conduction band (CB). These two states are calculated separately. The interaction of the electron in the CB and the hole left behind can significantly influence the final-state wave function and thus modify the ELNES spectra. The use of a super-cell minimizes the interactions between core–holes and the artificially imposed boundaries of the cell.

The final spectrum (the computed ELNES) is obtained by evaluating the strength of the transition between the initial and the final states in the dipole approximation. The matrix elements of transitions connecting the initial occupied states and the final unoccupied states are fully included in the transition-strength calculation [33]. This calculation ensures that the selection rule for the transition is automatically imposed; hence the states with appropriate angular momentum character are probed for different edges.

An alternative approach known as the equivalent-core approximation or $(Z+1)$-approximation [60–62] has also been used to take account of the core–hole effect. It is mainly used for calculations associated with the pseudo-potentials method when core electrons are excluded. The weakness of the $(Z+1)$ method is that it cannot distinguish core–hole effects in different states.

A reliable band-structure calculation using a large super-cell with the core–hole effect appears to be a good 'recipe' for ELNES calculations. Superior agreement between measured and calculated ELNES spectra has been shown by using the OLCAO band method with the implementation of the core–hole effect [59,63–72].

In the present study, experimental results for Al-$L_{2,3}$ and O-K ELNES of CA_2 and CA_6 crystals are compared with calculated near-edge structures to assign most of the significant spectral features to certain symmetry environments. This assignment should help the reader to establish analogies with other system of interest containing the same elements in the structure. The fine details of the spectra will be necessarily system specific. It should be noted that coordination is not the only factor that influences the ELNES structure; however, it will be a good starting point for interpretation.

2.5. Experimental procedure

A chemical-processing technique was used to synthesize pure crystalline CA_2 and CA_6 powders. The phase purity and crystallinity of the powders were confirmed by X-ray and TEM diffraction. Details of the powder preparation and characterization are explained elsewhere [73,74]. These powders were then crushed in pure, anhydrous ether and placed on a holey-carbon film on a copper TEM grid.

Energy-loss spectra were collected on a monochromated FEI Tecnai F20 G2 FEG microscope in STEM mode using a Gatan imaging filter (GIF Tridiem). Spectra were collected with a dispersion of 0.05 eV/channel and with an energy resolution determined by the full width at half maximum (FWHM) of the zero-loss peak (ZLP) of approximately 0.4 eV. For each phase, at least three particles were analyzed, and for each particle, five spectra were collected at the same location (no damage was observed). All the spectra were aligned on the energy scale with respect to their ZLP, and background subtracted using a power-law fit in the form of $A\exp(-E)$ [33]. Noise in the data was reduced using the 'smooth' function of digital micrograph after the background subtraction.

Electronic structure calculations were carried out for both CA_2 and CA_6 using the supercell OLCAO method, including the core–hole interactions as it was described in detail by Mo and Ching

[59], and Ching and Rulis [63]. Super-cells of 96 and 64 atoms for CA_2 and CA_6 were used (i.e., 8 and 2 formula units, respectively). The calculated edges are the weighted sum of the calculated spectra from crystallographically non-equivalent sites. The crystal orientation effects with respect to the electron beam direction were not considered. All calculations are based on the reported crystal structures of CA_2 and CA_6, there is no subsequent modeling or simulation involved. All the interactions up to atoms far beyond the nearest or next nearest neighbor atoms are all included. However, only the nearest neighbor or next-nearest neighbor coordination of the central atoms are compared for the interpretation of the edges in this study. The nearest-neighbor coordination of the atoms is determined based on the bond length criteria. If the bond length between Ca–O is less than 3.00 Å and the bond length between the Al–O is less than 2.20 Å, they are considered to be a member of coordination polyhedra. The bond lengths between the coordinated atoms based on these criteria are given in Table 5.

Table 5
Structural information and data used for calculations.

	CA_2	CA_6
Ca–O bond length (Å) Number in { } implies the number of such bonds to each Ca	Ca–O(2)=2.0795 {2} Ca–O(2)=2.3905 {2} Ca–O(3)=2.6025 {2}	Ca–O(3)=2.7828 {6} Ca–O(5)=2.7117 {6}
Al-O Bond length (Å) Number in { } implies the number of such bonds to each Al	Al(1)–O(2)=1.7437 Al(1)–O(2)=1.7544 Al(1)–O(3)=1.7297 Al(1)–O(4)=1.7878 Al(2)–O(1)=1.7165 Al(2)–O(3)=1.7151 Al(2)–O(4)=1.7777 Al(2)–O(4)=1.8070	Al(1)–O(4)=1.8791{6} Al(2)–O(1)=2.0409 Al(2)–O(3)=1.7515 {3} Al(3)–O(2)=1.8103 Al(3)–O(4)=1.7954 {3} Al(4)–O(3)=1.9536 {3} Al(4)–O(5)=1.8756 {3} Al(5)–O(1)=1.8433 Al(5)–O(2)=1.9855 Al(5)–O(4)=1.9993 {2} Al(5)–O(5)=1.8062 {2}

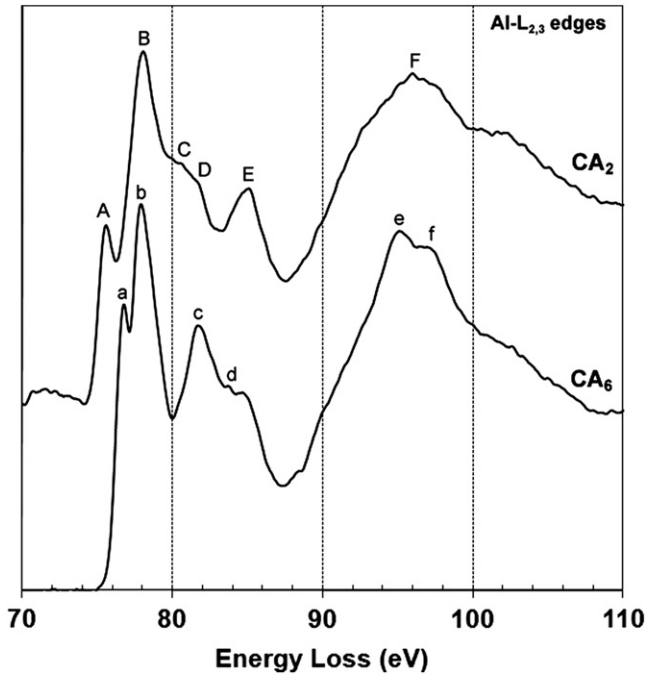

Fig. 1. Experimentally measured Al-$L_{2,3}$ edges from CA_2 and CA_6 powders. Features A–F and a–f are discussed in the text.

3. Results

In this study, the O-K and Al-$L_{2,3}$ edges of CA_2 and CA_6 crystals were examined in detail. The fine structure in these spectra arises from the transition of an electron from a core level to an unoccupied state lying above the Fermi level [36]. For example, the K edge results from excitations of 1*s* electrons into unoccupied 2*p* states, in accordance with the dipole selection rules. Similarly, the $L_{2,3}$ edges result from transitions between 2*p* states to 3*d* states. If a large collection aperture is used, dipole-forbidden transitions can sometimes be observed [33], but this is not the case for the spectra shown in this report.

3.1. Experimentally measured ELNES

Fig. 1 shows experimentally measured Al-$L_{2,3}$ edges from CA_2 and CA_6 powders. These spectra were collected in random crystal orientations; no special zone axis orientations were intended. The Al-$L_{2,3}$ near-edge structures of CA_2 and CA_6 show several distinct features. These features are labeled with letters from A to F and a to f in Fig. 1 and their energies are given in Table 6. These energy values correspond to the possible peak positions and will be used to compare the peak positions of CA_2 and CA_6 phases with respect to each other on the energy scale. In this study, Al-L_2 and Al-L_3 edges were not distinguished and they were treated as one edge structure since the spin–orbit effect in Al is negligible.

The O-K near-edge structures of CA_2 and CA_6 are shown in Fig. 2. These structures also reveal several different features labeled with roman numerals, which indicate O sites with different nearest neighbor (NN) and next nearest neighbor (NNN) coordinations. While the O-K edge of CA_6 shows one low-energy shoulder peak (I), one broad second peak (II) and several smaller peaks at higher energies, the O-K edge of CA_2 has two major peaks with similar intensities (i and iv). The energies, which correspond to the distinct features labeled in Fig. 2, are listed in Table 7. A pre-edge peak, several electron volts (~8 eV) before the threshold of the O-K edge, that is usually associated with electron-beam damage, was not observed for CA_2 and CA_6 O-K edges during acquisitions. CA ($CaAl_2O_4$) and some other complex oxides are known to suffer from beam damage and show this effect [22,75].

Table 6
Experimentally measured energies of the features in Al-$L_{2,3}$ edges in CA_2 and CA_6 powders.

CA_2 Al-$L_{2,3}$	A	B	C	D	E	F
(i)	75.7 ± 0.1	78.1 ± 0.1	80.8 ± 0.1	81.9 ± 0.1	85.2 ± 0.1	96.2 ± 0.1
CA_6 Al-$L_{2,3}$	a	b	c	d	e	f
(ii)	76.9 ± 0.1	78.1 ± 0.1	81.9 ± 0.1	84.5 ± 0.5	95.4 ± 0.1	97.4 ± 0.1

3.2. Calculated near-edge structures

Figs. 3 and 4 show the computed Al-$L_{2,3}$ edges for CA_2 and CA_6 crystals, respectively. In these figures, computed Al-$L_{2,3}$ edges for individual Al ions that sit in different symmetry environments and the weighted sum of these individually computed edges are shown together with the experimental Al-$L_{2,3}$ edges for later comparison.

Similarly, Figs. 5 and 6 show the computed O-K edges for CA_2 and CA_6 crystals, respectively. In these figures; computed O-K edges for individual O ions that sit in different symmetry environments and the weighted sum of these individually computed edges are shown together with the experimental O-K edges to facilitate the comparison.

The weighted sum edges given in Figs. 3–6 were assembled ignoring crystal orientation effects. All the computed curves were aligned on the energy scale with respect to the experimental curves and in order to compare the computed spectra with those measured experimentally, a Gaussian broadening function was included in the calculation. Although the energy resolution (FWHM) of all experimental spectra was $\sim$0.4 eV, all the calculated near-edge structures were broadened by a Gaussian function of 1.0 eV; using a value of 0.4 eV would essentially only increase the noise of the calculated spectra.

4. Discussion

Calcium aluminate phases have very large and complicated unit cells. Although the unit cells of the calcium aluminate phases each contain only Ca, Al, and O ions, these ions have different local environment in each compound. Distinct spectral features observed in the experimental spectra are compared below to features in the calculated spectra in order to assign these features to a certain symmetry environment of the central ion and thus to create the fingerprint for particular compounds. Throughout the following discussion and for the computer calculations, it is assumed that the materials have the ideal and stoichiometric structures. As mentioned previously, although both experimental and calculated edges include information from interactions up to atoms far beyond the nearest or next-nearest neighbor atoms, the interpretation of the edges are based on the nearest-neighbor coordination assignments of the atoms. If the CaO bond length is <3.00 Å or the A–O bond length is <2.20 Å, the atoms are assumed to be coordinated. The local environment around the Al and O ions according to the bond length criteria are summarized below for CA_2 and CA_6 crystals.

In an ideal CA_2 crystal, the Al atoms are located in two different crystallographic locations. According to the bond length criteria used in this study, both of these Al atoms are

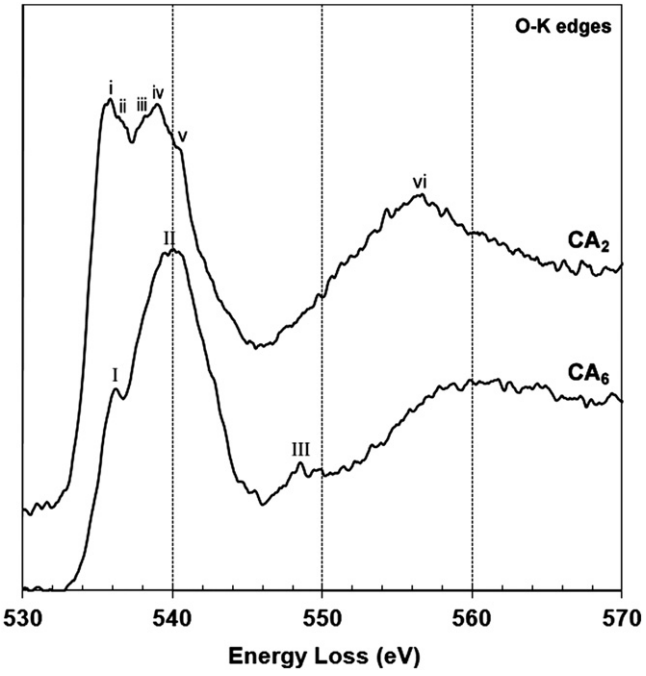

Fig. 2. Experimentally measured O-K edge from CA_2 and CA_6 powders. Features i–vi and I–III are discussed in the text.

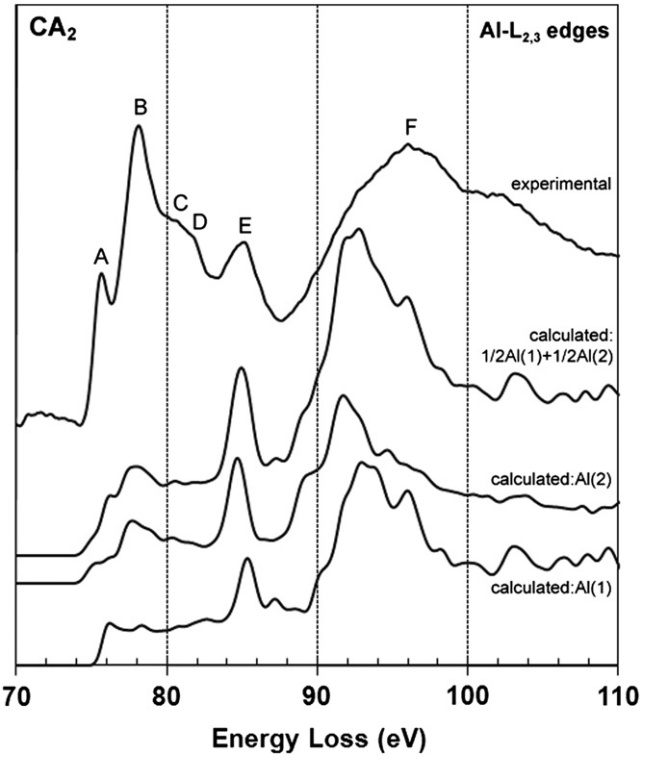

Fig. 3. Experimentally measured and theoretically calculated Al-$L_{2,3}$ edges from CA_2 powders.

Table 7
Experimentally measured energies (eV) of the features in O-K edges in CA_2 and CA_6 powders.

CA_2 O-K	i	ii	iii	iv	v	vi
(i)	535.8 ± 0.1	536.8 ± 0.3	538.2 ± 0.4	539.2 ± 0.2	540.6 ± 0.2	556.8 ± 0.2
CA_6 O-K	**I**	**II**	**III**	**IV**		
(i)	536.4 ± 0.2	540.2 ± 0.5	545.3 ± 0.5	548.7 ± 0.2		

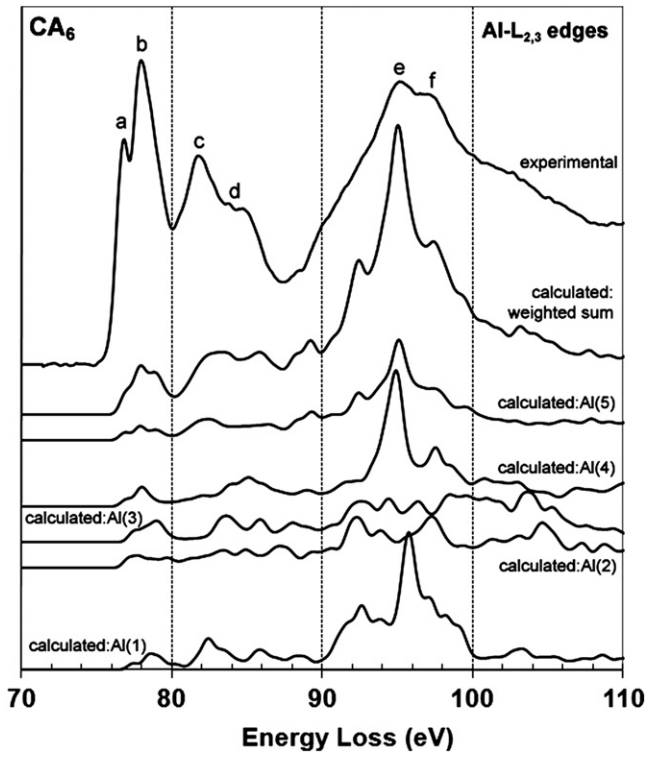

Fig. 4. Experimentally measured and theoretically calculated Al-$L_{2,3}$ edges from CA_6 powders.

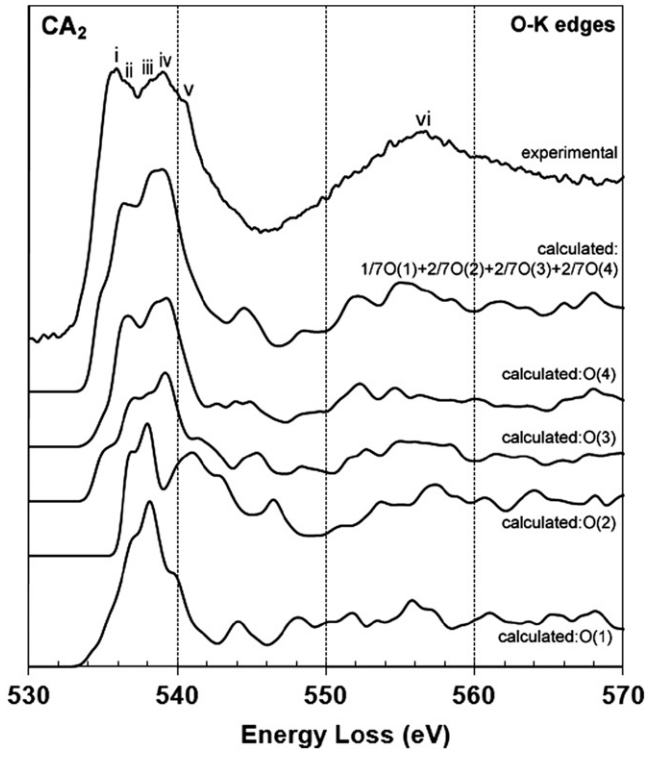

Fig. 5. Experimentally measured and theoretically calculated O-K edge from CA_2 powders.

tetrahedrally coordinated to the surrounding O atoms. Therefore, the experimentally measured Al-$L_{2,3}$ edge contains features, which correspond to the electronic transitions from both of these sites. Since there are equal numbers of Al(1) and Al(2) ions in a

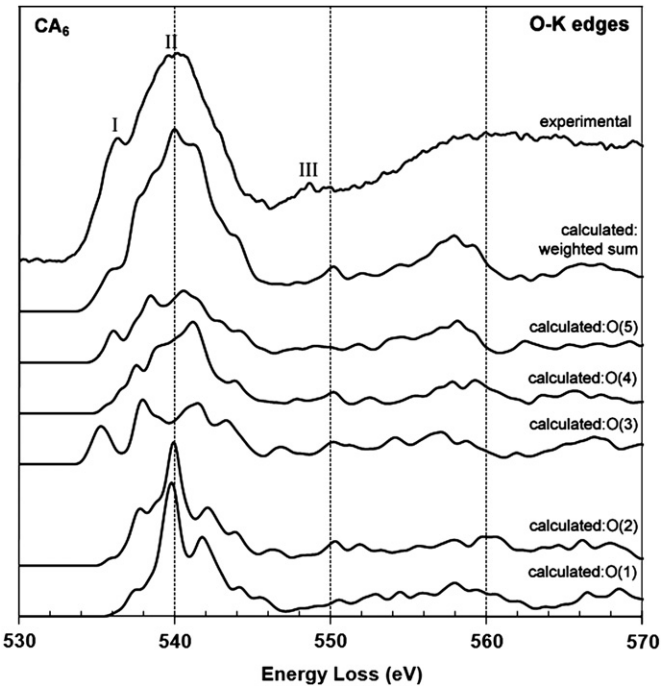

Fig. 6. Experimentally measured and theoretically calculated O-K edge from CA_6 powders.

CA_2 unit cell, the weighing factors for each Al ions are the same ($\frac{1}{2}$ Al(1) and $\frac{1}{2}$ Al (2)). The weighing factor of each individual ion is important because the calculated edges are the weighted sum of the individually calculated edges.

The ideal CA_6 unit cell contains Al atoms in five crystallographically different locations. While three of the Al atoms are octahedrally coordinated, two of the Al atoms are tetrahedrally coordinated to surrounding O atoms. The weighing factors for Al(1), Al(2), Al(3), Al(4), and Al(5) are 1/12, 1/12, 1/6, 1/6, and 1/2, respectively. It is known that in the CA_6 crystal one of the Al atoms is in the trigonal bi-pyramidal site which has 5- fold coordination. However, according to the bond-length criteria used in this study for the interpretation of the edges, the Al atom which sits in the trigonal bi-pyramidal site is treated as 4-fold throughout the discussion.

The site symmetries for O ions are more complicated since there are two types of cations present in CA_2 and CA_6 unit cells. In an ideal CA_2 unit cell there are four different O sites. O(1) is coordinated with four Al atoms, O(2) is coordinated with two Al and two Ca atoms. Each of the other two O atoms has three nearest neighbors instead of four: of these, O(3) is coordinated with two Al atoms and one Ca atom, while O(4) is coordinated with three Al atoms. The weighing factors for O(1), O(2), O(3) and O(4) are 1/7, 2/7, 2/7, and 2/7, respectively.

The ideal CA_6 structure contains five different O sites. Three of the O atoms; O(1), O(2), and O(4); are coordinated with four Al atoms, O(3) can be assumed to be coordinated with four Al and 2 Ca atoms and O(5) is coordinated with three Al atoms and one Ca atom, according to the coordination definitions reported earlier. The weighing factors for O(1), O(2), O(3), O(4), and O(5) are 2/19, 2/19, 3/19, 6/19, and 6/19, respectively.

4.1. ELNES at Al-$L_{2,3}$ edges

The Al near-edge structure of CA_2 contains signals originating from two different Al sites with solely tetrahedral (4-fold)

coordination. However, the Al near-edge structure of CA_6 contains signals from five different Al sites with both 4- and 6-fold symmetry environments. When the experimental spectra from the Al-$L_{2,3}$ edges of CA_2 and CA_6 structures are compared (Fig. 1), the distinct features in each spectrum show the differences in the local environments of the Al atoms in each unit cell. Although several features of the experimental spectra for CA_2 and CA_6 structures are at similar energies (Table 6), the small-scale differences do not make it possible to assign a feature to a specific coordination just by comparing these two experimental spectra. One approach that can help to isolate the features coming from tetrahedrally coordinated Al atoms and octahedrally coordinated Al atoms in CA_6 is to investigate the materials with the same elemental make-up which contain only Al ions that are octahedrally (6-fold) coordinated with oxygen ions [41]. Unfortunately, there are no calcium aluminate phases with the same elemental make-up that have Al atoms only in the octahedral oxygen coordination. In this case, the interpretation of these experimental spectra can be greatly facilitated with the help of theoretical calculations.

In Fig. 3 calculated ELNES of Al(1) and Al(2) ions from CA_2 are plotted together with the weighted sum of these two sites. All the calculated spectra are aligned on the energy scale in such a way that the best match between the experimental and calculated (weighted-sum curve) curves is achieved. The weighted sum of the calculated Al-$L_{2,3}$ edges from two crystallographically non-equivalent Al sites Al(1) and Al(2) in CA_2 reproduces all the features of the experimental spectrum at the correct energies except for the last broad peak. However, the intensity distributions of the features differ from the experimental data. In particular, the intensity of the second peak in experimental spectrum labeled as 'B' is underestimated in the calculated spectrum. Other groups have similarly reported underestimations of the peak intensity around the spectral threshold [59,67,76,77]. At the present time, the origin of such discrepancies are disputed; however, it may be related to excitonic effects along with other effects. A more rigorous inclusion of such effect in the present methodology has not been worked out yet. The inclusion of many body effects are very demanding and has only been applied to crystals with simpler structures such as LiF, h-BN, and diamond [78,79]; only recently Olovsson et al. reported that underestimation of peak intensities also appear in Mg-$L_{2,3}$ edge in MgO [80].

As it is shown in Fig. 3, the calculated ELNES of Al(1) and Al(2) present some significant differences although both Al(1) and Al(2) ions are tetrahedrally coordinated with the surrounding O ions in CA_2 crystal. These differences are mainly due to the differences in bond lengths between Al–O ions (Table 5) and/or due to the differences on the nearest neighbor oxygen atoms.

Fig. 4 shows the calculated Al-$L_{2,3}$ edge of CA_6 which is the weighted sum of 1/4 Al_{tet} and 3/4 Al_{oct} sites. Individually calculated Al-$L_{2,3}$ edges of CA_6 are also shown in the same figure for a comprehensive comparison. Although calculations for the Al-$L_{2,3}$ edges of CA_6 predicted some of the features in the experimental spectrum, the match is not as good as it is for CA_2. A possible reason is that the size of the supercell in the CA_6 calculation was the same as the unit cell (64 atoms, 2 formula units) which might be too small to fully avoid the core–hole/core–hole interaction. The next level of supercell ($2 \times 2 \times 1$) would need 256-atom cell which was too large to carry out the calculations at the present time. In CA_2 the supercell used was 96 atoms that correspond to 2 unit cells and 8 formula units which is larger than what could be used for CA_6.

It is also possible that the crystallography (orientation of the grain) plays a role in determining the collection efficiency of certain sites in layered structures [81]. CA_6 has a layered structure, which may cause the measurements to be skewed towards one site or to introduce directional effects on cross sections of certain sites. When the EELS data were acquired, the orientation of the grains was not determined or controlled. When the crystal is non-polar or has some type of directionality, then the spectra obtained can have different peak intensities, etc., depending on the orientation and the size of the collection aperture. In principle, it is possible to look into the orientation dependence of the spectrum [71]. However, in the present work with more complicated structures, this point is left to a future investigation.

When the calculated curves from individual Al(1), Al(2), Al(3), Al(4), and Al(5) in the CA_6 crystal are compared with each other, it can be seen that the curves from the tetrahedrally coordinated Al ions (Al(2) and Al(3)) are significantly different than the curves calculated for octahedrally coordinated Al ions (Al(1), Al(4), and Al(5)). These differences illustrate the effect of the site symmetries on the near-edge structures. Although the curves from Al(2) and Al(3) or the curves from Al(1), Al(4), and Al(5) are also different than each other due to the difference in the bond lengths, the outline of the curves are similar. In Fig. 4, when these calculated curves from individual Al ions are compared with the experimental curve, it appears that the peak labeled as 'e' in the experimental spectrum is mainly coming from the octahedrally coordinated Al ions. However, for the rest of the peaks in the experimental spectrum, it is not trivial to assign the peaks to certain symmetry environments even with the help of the calculated curves.

It should also be noted that although the comparison in this study are mainly based on the Al–O interactions, the near-edge structure associated with a cation in a mixed oxide can also be affected by the presence of other cations. One of the possible reasons for multiple cation effect in Al-$L_{2,3}$ is that the *p*-type states of Al in the conduction band are more delocalized and therefore more sensitive to the multiple ion effect.

4.2. ELNES at O-K edges

The experimental O-K near-edge structures are distinctly different for CA_2 and CA_6 (Fig. 2 and Table 7). This clear difference can be linked to the very different ionic environments in CA_2 and CA_6 crystals. There are four crystallographically different O sites in the CA_2 and five crystallographically different O sites in the CA_6 structure. Since both crystals have several different coordinations for the O atoms in their structures, it is not possible to assign features in the spectra to certain symmetry environments by just comparing the experimentally measured O-K edges of CA_2 and CA_6. In order to interpret the O-K edge in both structures meaningfully, a comparison with computed spectra are essential.

In Fig. 5, spectra from the calculated O-K edges from individual O ions that sit in different symmetry environments in CA_2 are plotted together with the weighted-sum spectrum of these individual spectra. This sum spectrum is the summation of the $\frac{1}{7}$ O(1), $\frac{2}{7}$ O(2), $\frac{2}{7}$ O(3) and $\frac{2}{7}$ O(4) sites. All the calculated spectra are aligned on the energy scale in such a way that the best match between the experimental and calculated (weighted-sum curve) curves is achieved. Fig. 5 shows that the experimental O-K edge of the CA_2 is in good agreement with the weighted sum of the calculated spectrum. The energies of most features in the calculated O-K edge match well with the experimental spectrum and there is a reasonable correlation between the calculated and measured relative intensities.

When the experimental O-K edge of CA_2 is compared with the O-K edges from the O(1), O(2), O(3), and O(4) sites individually, it appears that peaks labeled as 'iii' and 'iv' in the experimental spectrum are dominated by O(3) and O(4) sites. Both O(3) and

O(4) have three nearest neighbors around them. O(3) is coordinated with 2Al and 1Ca ions and O(4) is coordinated with 3Al ions.

Fig. 6 shows the experimental and calculated O-K edges of the CA_6 crystal. Similar to the results of the Al-$L_{2,3}$ edges, the match between the calculated and experimental O-K edge of CA_6 is not as good as the match between the calculated and experimental O-K edge of CA_2. It is believed that again the size of the CA_6 supercell used for the calculations and/or the effect of the crystal orientation could be responsible for this observation. It may also be relevant that the magnetoplumbite structure of CA_6 is closely related to that of the β-aluminas. β-Aluminas are well known as ionic conductors since the alkali ion (usually Na^+ or K^-) present in their structure moves quite readily. The possibility that movement of the Ca^{2+} ions (as occurs during e-beam irradiation of certain compounds like calcium aluminate and calcium silicate hydrates) may influence the ELNES has not been explored. This is then a consequence of the concern that locally, the structure is not the 'known' crystal structure. This topic is still actively being examined for many materials with a closely related crystal structure [82]. It should be noted that structures used in the calculations are assumed to be perfect crystals. However, it may not be the case for the CA_6 crystals prepared via chemical processing or under the e-beam.

The O-K edge of CA_6 is coming from five different oxygen sites and the site frequencies of these five different oxygen ions in CA_6 (the weighting factors) are in the ratio of 2:2:3:6:6. In Fig. 6, calculated O-K edges from different oxygen sites are also shown in order see the effects of different symmetry environment around the same anion in the same crystal. When these individual spectra from different oxygen sites are compared, it can be seen they all give rise to slightly different features at similar energy loss values. The differences in their spectra originate in their different local bonding configuration. For example, although oxygen ions O(2) and O(4) are both coordinated with 4 Al ions, their dissimilar calculated spectra reflects very well the differences in their local bonding symmetry. As listed in Table 5, O(4) has a shorter Al–O bond of 1.795 Å than O(2).

5. Conclusions

The ELNES of the Al-$L_{2,3}$ and O-K edges of CA_2 and CA_6 were measured. The same edge structures were also calculated theoretically using the OLCAO method, including the core–hole effect. There is quite a good agreement between the experimentally measured and theoretically calculated spectra for the CA_2 and CA_6 structures. The reason the agreement for the CA_6 structure is less good can mainly be due to the very directional crystallography of the CA_6 crystal. However, the fingerprint approach can still be applied.

A comparison of the experimental spectra of both structures and the calculated ELNES spectra facilitates the interpretation of the near-edge structures. Especially, the calculated ELNES from individual cation or anion sites with different local environment are used to assign the spectral features to certain local symmetries. This procedure is very helpful for determining the fingerprints of the structures. By comparing these fingerprints two phases can be distinguished from one another even though they contain the same chemical species. Due to the high spatial resolution of the technique, ELNES fingerprints can be used to study the chemistry and the structure of the nanomaterials, and 'phases' that are confined to interfaces or grain boundaries. Distinct spectral features in the experimentally measured ELNES spectra can be assigned to certain symmetry environments with the help of calculated spectra. Such features can be used to understand the local atomic arrangements in unknown structures involving the same constituent atoms.

Acknowledgments

The authors are grateful to Dr. Nigel Browning and Ms. Miaofang Chi for their help with ELNES measurements. The work was initially supported by the US Department of Energy (Grant DE-FG02-01ER45883) and an NSF international travel (Grant INT-0322622). Subsequent support was provided by the 3M Harry Heltzer Endowed Chair funds at the University of Minnesota. The authors acknowledge use of facilities at the National Center for Electron Microscopy, Lawrence Berkeley Lab, which is supported by the US Department of Energy under Contract #DE-AC02-05CH11231. I.A. acknowledges funding from Sandia's Truman Fellowship LDRD. WYC is supported by the US DOE under Grant #DE-FG02-84DR45170. This research used resources of NERSC supported by Office of Science of DOE under Contract #DE-AC03-76SF00098.

References

[1] J. Bied, 320290, 391454, 1908.
[2] E.S. Shepherd, G.A. Rankin, F.E. Wright, Am. J. Sci. 28 (1909) 293–333.
[3] M.E. Lines, J.B. MacChesney, K.B. Lyons, A.J. Bruce, A.E. Miller, K. Nassau, J. Non-Cryst. Solids 107 (1989) 251–260.
[4] H.C. Hafner, N.J. Kreidl, R.A. Weidel, J. Am. Ceram. Soc. 41 (8) (1958) 315–323.
[5] F.T. Wallenberger, N.E. Weston, S.A. Dunn, J. Non-Cryst. Solids 124 (1) (1990) 116–119.
[6] H. Hosono, K. Yamazaki, Y. Abe, J. Am. Ceram. Soc. 68 (11) (1985) C304–C305.
[7] S. Jonas, F. Nadachowski, D. Szwagierczak, Ceram. Int. 25 (1) (1999) 77–84.
[8] M.P. Mallamaci, K.B. Sartain, C.B. Carter, Philos. Mag. A 77 (3) (1998) 561–575.
[9] M.K. Cinibulk, R.S. Hay, J. Am. Ceram. Soc. 79 (5) (1996) 1233–1246.
[10] M. Lacerda, J.T.S. Irvine, F.P. Glasser, A.R. West, Nature 332 (1988) 525–526.
[11] K. Hayashi, S. Matsuishi, T. Kamiya, M. Hirano, H. Hosono, Nature 419 (6906) (2002) 462–465.
[12] P.B. Braun, Philips Res. Rep. 12 (1957) 491–548.
[13] A. Utsunomiya, K. Tanaka, H. Morikawa, F. Marumo, H. Kojima, J. Solid State Chem. 75 (1988) 7–200.
[14] N. Iyi, S. Takekawa, S. Kimura, J. Solid State Chem. 83 (1989) 8–19.
[15] B. Cockayne, D.S. Robertson, Solid State Commun. 2 (11) (1964) 359–360.
[16] D.W. Goodwin, A.J. Lindop, Acta Crystallogr. B26 (1970) 1230–1235.
[17] E.R. Boyko, L.G. Wisnyi, Acta Crystallogr. 11 (1958) 444–445.
[18] K.J.D. MacKenzie, M. Schmucker, M.E. Smith, I.J.F. Poplett, T. Kemmitt, Thermochim. Acta 363 (2000) 181–188.
[19] C. Gervais, K.J.D. MacKenzie, M.E. Smith, Magn. Reson. Chem. 39 (2001) 23–28.
[20] C. Weigel, G. Calas, L. Cormier, L. Galoisy, G.S. Henderson, J. Phys.: Condens. Matter 20 (2008) 135219.
[21] G.S. Henderson, D.R. Neuville, L. Cormier, Can. J. Chem. 85 (2007) 801–805.
[22] N. Jiang, J. Appl. Phys. 100 (2006) 0137031–0137038.
[23] B. Tavasci, Tonindustrie-Zeitung 61 (1937) 729–731.
[24] K. Lagerqvist, S. Wallmark, A. Westgren, Z. Anorg. Chem. 234 (1937) 1.
[25] J.R. Goldsmith, J. Geol. 56 (1948) 80.
[26] C. Goria, A. Burdese, La Ricerca Scientifica 21 (1951) 1613.
[27] N.E. Filonenko, I.V. Laurov, J. Appl. Chem. (USSR) 23 (1950) 1040.
[28] R.W. Nurse, J.H. Welch, A.J. Majumdar, Br. Ceram. Trans. 64 (9) (1965) 409–418.
[29] H. Curien, C. Guillemin, J. Orcel, M. Sternberg, C. R. Acad. Sci. Paris 242 (1956) 2845–2847.
[30] K. Kato, H. Saalfeld, Neues. Jahrb. Min. Abh. 109 (1968) 192–200.
[31] R. Collongues, D. Gourier, A. Kahn-Harari, A.M. Lejus, J. Thery, D. Vivien, Annu. Rev. Mater. Sci. 20 (1990) 51–82.
[32] K. Kimura, M. Ohgaki, K. Tanaka, H. Morikawa, F. Marumo, J. Solid State Chem. 87 (1990) 186–194.
[33] R.F. Egerton, in: Electron Energy-Loss Spectroscopy in the Electron MicroscopePlenum Press, New York, 1996.
[34] P. Rez, D.A. Muller, Annu. Rev. Mater. Res. 38 (2008) 535–558.
[35] R. Brydson, in: Electron Energy Loss SpectroscopyGarland Science, 2001.
[36] D.B. Williams, C.B. Carter, in: Transmission Electron Microscopy: A Textbook for Materials Science, second ed., Plenum Press, New York, 2009.
[37] R. Brydson, B.G. Williams, H. Sauer, W. Engel, R. Schlogl, M. Muller, E. Zeitler, J.M. Thomas, J. Chem. Soc. Faraday Trans. 1 84 (1988) 631–646.
[38] F. Hofer, P. Golob, Ultramicroscopy 21 (1987) 379–384.
[39] J. Tafto, O.L. Krivanek, Phys. Rev. Lett. 48 (1982) 560–563.
[40] R.D. Leapman, L.A. Grunes, P.L. Fejes, Phys. Rev. B 26 (1982) 614–635.

[41] M.A. Gülgün, W.Y. Ching, Y.-N. Xu, M. Ruhle, Philos. Mag. B 79 (1999) 921–940.
[42] R. Brydson, J. Microsc. 180 (1995) 238–249.
[43] L.A.J. Garvie, A.J. Craven, R. Brydson, Am. Mineral. 79 (1994) 411–425.
[44] S.D. Berger, D.R. McKenzie, P.J. Martin, Philos. Mag. Lett. 57 (1988) 285–290.
[45] J. Bruley, D.B. Williams, J.J. Cuomo, D.P. Pappas, J. Microsc. 180 (1995) 22–32.
[46] L.A.J. Garvie, A.J. Craven, R. Brydson, Am. Mineral. 80 (1995) 1132–1144.
[47] P.L. Hansen, D.W. McComb, R. Brydson, Micron Microsc. Acta 23 (1992) 169–172.
[48] J.H. Paterson, O.L. Krivanek, Ultramicroscopy 32 (1990) 319–325.
[49] R.D. Leapman, P.L. Fejes, J. Silcox, Phys. Rev. B 28 (1983) 2361–2373.
[50] R. Brydson, J. Phys. D 29 (1996) 1699–1708.
[51] V. Serin, C. Colliex, R. Brydson, S. Matar, F. Boucher, Phys. Rev. B 58 (1998) 5106–5115.
[52] J.J. Rehr, R.C. Albers, Rev. Mod. Phys. 72 (2000) 621–654.
[53] A. Filipponi, A. Di Cocco, C.R. Natoli, Phys. Rev. B 52 (1995) 15122–15134.
[54] S. Kostlmeier, C. Elsasser, Phys. Rev. B 60 (1999) 14025–14034.
[55] P. Rez, L.J. Alvarez, C. Pickard, Ultramicroscopy 78 (1999) 175–183.
[56] W.Y. Ching, J. Am. Ceram. Soc. 73 (1990) 3135–3160.
[57] S.-D. Mo, W.Y. Ching, R.H. French, J. Phys. D 29 (1996) 1761–1766.
[58] S.-D. Mo, Y.-N. Xu, W.Y. Ching, J. Am. Ceram. Soc. 80 (1997) 1193–1197.
[59] S.-D. Mo, W.Y. Ching, Phys. Rev. B 62 (2000) 7901–7907.
[60] M.M. Disko, J.C.H. Spence, O.F. Sankey, D. Saldin, Phys. Rev. B 33 (1986) 5642–5651.
[61] K. Lie, R. Brydson, H. Davock, Phys. Rev. B 59 (1999) 5361–5367.
[62] T. Mizoguchi, I. Tanaka, F. Oba, K. Ogasawara, H. Adachi, Phys. Rev. B 61 (2000) 2180–2187.
[63] W.Y. Ching, P. Rulis, J. Phys.: Condens. Matter 21 (2009) 104202-101-16.
[64] S.D. Mo, W.Y. Ching, Phys. Rev. B 62 (2002) 7901–7907.
[65] I. Tanaka, T. Mizoguchi, T. Yamamoto, J. Am. Ceram. Soc. 88 (2005) 2013–2029.
[66] I. Tanaka, T. Mizoguchi, T. Sekine, H. He, K. Kimoto, S.D. Mo, W.Y. Ching, Appl. Phys. Lett. 78 (15) (2001) 2134–2136.
[67] S.D. Mo, W.Y. Ching, Appl. Phys. Lett. 78 (15) (2001) 3809–3911.
[68] W.Y. Ching, S.D. Mo, Y. Chen, J. Am. Ceram. Soc. 85 (1) (2002) 11–15.
[69] Y.N. Xu, S.D. Mo, Y. Chen, W.Y. Ching, Phys. Rev. B 65 (2002) 235105/1–235105/4.
[70] I. Tanaka, T. Mizuguchi, M. Matsui, S. Yoshioka, H. Adachi, T. Yamamoto, T. Okajima, M. Umesaki, W.Y. Ching, Y. Inoue, M. Mizuno, H. Araki, Y. Shirai, Nat. Mater. 2 (8) (2003) 541–545.
[71] T. Mizoguchi, I. Tanaka, S. Yoshioka, M. Kunisu, T. Yamamoto, W.Y. Ching, Phys. Rev. B70 (2004) 045103.
[72] P. Rulis, W.Y. Ching, M. Kohyama, Acta Mater. 52 (10) (2004) 30009–30018.
[73] A. Altay, Calcium aluminate in alumina, Ph.D., University of Minnesota, Minneapolis, 2006.
[74] A. Altay, C.B. Carter, I. Arslan, M.A. Gülgün, Philos. Mag. 89 (7) (2009) 605–621.
[75] N. Jiang, J.C.H. Spence, Ultramicroscopy 106 (2006) 215–219.
[76] K. Kimoto, Y. Matsui, T. Nabatame, T. Yasuda, T. Mizoguchi, I. Tanaka, A. Toriumi, Appl. Phys. Lett. 83 (21) (2003) 4306–4308.
[77] T. Mizoguchi, I. Tanaka, M. Kunisu, M. Yoshiya, H. Adachi, W.Y. Ching, Micron 34 (3-5) (2003) 249–254.
[78] E.L. Shirley, Phys. Rev. Lett. 80 (4) (1998) 794–797.
[79] J.A. Soininen, E.L. Shirley, Phys. Rev. B 64 (2001) 165112–165115.
[80] W. Olovsson, I. Tanaka, T. Mizoguchi, P. Puschnig, C. Ambrosch-Draxl, Phys. Rev. B 79 (4) (2009) 041102(R)-1-4.
[81] S. Turan, C.A. Davis, K.M. Knowles, Inst. Phys. Conf. Ser. 147 (2) (1995) 63–66.
[82] Z. Zhang, Y. Zhang, X. Li, J. Xu, Y. Huang, J. Non-Cryst. Solids 354 (2008) 1943–1947.